ORGANOMETALLICS

pubs.acs.org/Organometallics Article

Electrochemical Reduction Mechanism of $[(\eta^5\text{-}C_5H_5)Fe(dppf)(CO)]^+$ (dppf = 1,1′-Bis(diphenylphosphino)ferrocene)

Yixian Pan, Marc Schnierle, Daniel Auweiler, and Mark R. Ringenberg*

Cite This: *Organometallics* 2021, 40, 760−765

Read Online

ACCESS | Metrics & More | Article Recommendations | SI Supporting Information

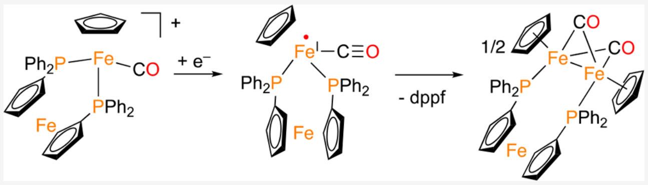

ABSTRACT: The complex $[CpFe(dppf)(CO)][B(Ar^F)_4]$ [**1**][$B(Ar^F)_4$] (Cp = cyclopentadienyl, dppf = 1,1′-bis(diphenylphosphino)ferrocene, and $[B(Ar^F)_4]^-$ = tetrakis[3,5-bis(trifluoromethyl)phenyl]borate) was made by removal of one carbonyl ligand from the dicarbonyl complex $[CpFe(CO)_2(\kappa^1\text{-dppf})]I$ and exchange of the I^- for $[B(Ar^F)_4]^-$ that allowed for electrochemical investigations. The cyclic voltammogram of $[\mathbf{1}]^+$ showed a reversible anodic process due to oxidation of the ferrocenediyl moiety of the dppf ligand. A quasi-reversible cathodic process was also observed, and this reduction occurred at the CpFe moiety, as determined by variable-temperature (+22 and −30 °C) IR spectroelectrochemistry (SEC) and further supported by DFT calculations. This reduction event resulted in the formation of the two possible dimers $[Cp_2Fe_2(\mu\text{-}CO)_2(\mu\text{-dppf})]$ and $[Cp_2Fe_2(CO)_2(\mu\text{-dppf})]$ along with deligation of one dppf ligand.

■ INTRODUCTION

The CpFe and Cp*Fe (Cp = cyclopentadienyl and Cp* = pentamethylcyclopentadienyl) organometallic moieties can exist in a range of stable redox states: i.e., Fe^{III}, Fe^{II}, and Fe^{I}.[1−5] The work by Lapinte and co-workers has shown that the redox chemistry of $[Cp(^*)Fe(L)_3]^n$ (L = mono- or bidentate phosphine ligands, CO ($n = +1$) or one X ligand ($n = 0$) such as ⁻OTf, Me, halides), especially reduction, causes dramatic changes in the coordination geometry where even bidentate phosphine ligand dechelation has been described.[1−4] Their study on $[CpFe(dppe)(CO)]^+$ and $[Cp^*Fe(dppe)(CO)]^+$ (dppe = 1,2-bis(diphenylphosphino)ethane), for example, found that the complex could be reduced by 1e⁻ to form the 19e⁻ Fe^I complex followed by dechelation of the dppe to give a 17e⁻ species (Scheme 1).[4] This Fe^I species then abstracted a H atom to form the iron hydride; this hydride could also be made directly by the addition of a hydride ligand (Scheme 1).

We report herein the straightforward[6] synthesis of $[CpFe(dppf)(CO)][B(Ar^F)_4]$ ([**1**][$B(Ar^F)_4$], dppf = 1,1′-bis(diphenylphosphino)ferrocene) and improved the solubility of the cationic complex through the exchange of the I^- counterion with the weakly coordinating, non-redox-active tetrakis[3,5-bis(trifluoromethyl)phenyl]borate $[B(Ar^F)_4]^-$. This salt exchange offered the ability to perform electrochemical studies on [**1**][$B(Ar^F)_4$]. The location of the redox events and the electrochemical mechanism were both determined through the use of spectroelectrochemistry. The spectroscopic observations were then further supported by molecular models determined by DFT calculations.

Scheme 1. Reactive Pathways of $[CpFe(CO)(dppe)]^+$ or $[Cp^*Fe(CO)(dppe)]^+$ with Reductants or H^-

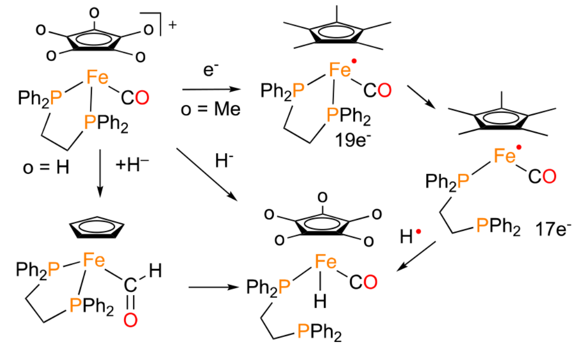

■ RESULTS AND DISCUSSION

The complex [**1**][$B(Ar^F)_4$] was synthesized by starting from $[CpFe(CO)_2I]$ followed by the addition of 1,1′-bis(diphenylphosphino)ferrocene (dppf) in EtOH under an inert atmosphere to yield the previously reported species $[CpFe(CO)_2(\kappa^1\text{-dppf})]I$,[6,7] as shown by IR spectroscopy (Figure S7). After the solution was heated to 160 °C in a microwave reactor, the dark red solution was treated with Et_2O and the dark orange solid was collected followed by

Received: January 7, 2021
Published: March 4, 2021

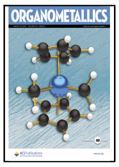

https://dx.doi.org/10.1021/acs.organomet.1c00010

crystallization from CH_2Cl_2/*n*-hexane. The I^- was exchanged for $[B(Ar^F)_4]^-$ by dissolving both solids in MeOH followed by precipitation with H_2O to yield [**1**]$[B(Ar^F)_4]$ (Scheme 2) The IR spectrum of [**1**]$[B(Ar^F)_4]$showed one CO band at 1967 cm^{-1}, and the compound [**1**]I showed a band at 1965 cm^{-1} (Figure S7).

Scheme 2. Synthesis of [1]$[B(Ar^F)_4]$ from $[CpFeCO_2]_2$.

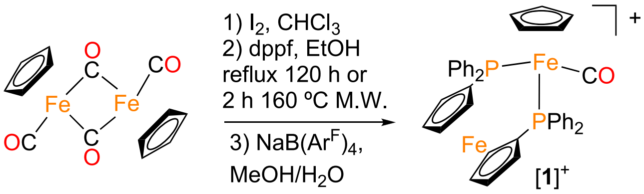

The molecular structure of [**1**]$[B(Ar^F)_4]$ is shown in Figure 1, and there were only minor differences from the reported [**1**]I; notably there is a tiny difference in the Fe−C and C−O distances of the bound carbonyl (Table 1).[7] The geometry around the Fe1 (distal) center shows the expected three-legged piano-stool geometry. The value d_{Fe-Fe} = 4.253 Å is likely outside the range for a M−M interaction.[8] The isostructural ruthenium analogue $[CpRu(dppr)(CO)]^+$ has also been reported and showed a longer M−M distance: d_{Ru-Ru} = 4.389 Å.[9] The Cp ligands at the proximal iron in dppf are in an eclipsed configuration with the dihedral angle P1−C1−C2−P2 = 5.78°. The UV−vis−NIR spectrum showed a band at λ_{max} = 405 nm and it was assigned using time-dependent (TD) DFT as a metal−ligand charge transfer (MLCT).

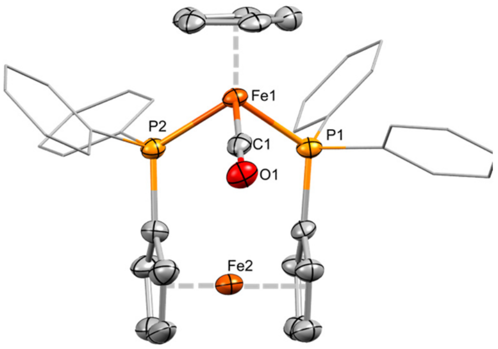

Figure 1. Molecular structure of [**1**]$[B(Ar^F)_4]$ determined from a crystallographic analysis. Thermal ellipsoids are shown at 50% probability; the $[B(Ar^F)_4]^-$ counterion and hydrogen atoms are omitted and phenyl rings presented in stick format for clarity. Crystallographic data are given in the Supporting Information.

Table 1. Selected Bond Distances and Anglesof $[1]^+$ (Å)

	X-ray $[1]^+$	[1]I[7]	$[1]^+$ DFT[a]
	Bond Distances (Å)		
Fe1−Fe2	4.253	4.246	4.227
Fe1−C1	1.736(5)	1.77(1)	1.749
C1−O1	1.162(5)	1.13(1)	1.148
Fe1−P1	2.2277(13)	2.236(3)	2.252
Fe1−P2	2.2441(14)	2.249(3)	2.258
	Bond Angles (deg)		
P1−Fe1−P2	101.24(5)	100.06(10)	96.93
Fe1−C1−O1	177.7(4)	173.4(9)	173.42
	Torsion Angle (deg)		
P1−C31−C36-P2	5.78	5.94	4.64

[a] B3LYP/def2-TZVP/J level of theory. Details are given in the Experimental Section, and full coordinates are provided as xyz files.

With the molecular structure of $[1]^+$ as a starting point, a geometry optimized model was generated from DFT calculations. The frontier Kohn−Sham molecular orbitals for $[1]^+$ are depicted in Figure 2. The highest occupied molecular orbital (HOMO) is located on the proximal iron (Fe2) of the ferrocenediyl moiety of the dppf ligand (Figure 2). The lowest unoccupied molecular orbital (LUMO) is an antibonding orbital between the distal iron (Fe1) and Cp ligand/P dative bonds and no contribution from the π* of the CO ligand (Figure 2). The calculated bond distances are in good agreement with the molecular structure determined by crystallographic analysis (Table 1).

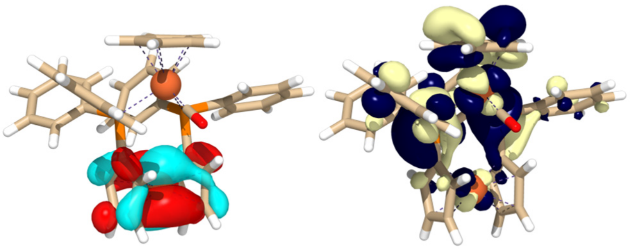

Figure 2. Depiction of restructured Kohn−Sham orbitals for the HOMO (turquoise/red) and LUMO (yellow/blue) determined from DFT calculations (B3LYP/def2-TZVP/J). Isosurface = 0.02.

The cyclic voltammogram (CV) of $[1]^+$ in 0.1 M n-$Bu_4NB(Ar^F)_4/CH_2Cl_2$ (this electrolyte/solvent combination was used in all further electrochemical based experiments found herein, including SEC) showed a reversible oxidation event at $E_{1/2}([1]^{+/2+})$ = 0.66 V vs $[FeCp_2]^{0/+}$, the internal standard for all potentials reported herein (Figures S1−S3). The Randles−Sevcik plot (Figure S4) shows a linear relationship between the square root of the scan rate and the current response for the first oxidation process, indicating that the process is under diffusion control.[10]

The location of the oxidization process was assigned to the ferrocenediyl moiety of the dppf ligand on the basis of the UV−vis−NIR spectroelectrochemistry (SEC) and IR SEC (Figures S9 and S11). The UV−vis−NIR SEC spectrum showed only two new weak bands at λ_{max} = 400 and 630 nm, consistent with dppf ligand oxidation.[11−14] The IR SEC spectrum showed only a minor change in $\nu_{CO}([1]+)$ = 1966 cm^{-1} to $\nu_{CO}([1]^{2+})$ = 1972 cm^{-1}, with $\Delta\nu_{CO}$ = 6 cm^{-1} (Figure S10).[15] The small $\Delta\nu$ is consistent with oxidation remote to the IR-active moiety, which was found to be the case for the dppf-substituted ruthenium metallacumulene chromophore $[TzRu(dppf)(C{=}C{=}CPh_2)]^+$ (Tz = tris(pyrazolyl)borate), where dppf oxidation resulted in $\Delta\nu_{CC}$ = 15 cm^{-1}.[14,16] DFT calculations also supported the dppf oxidation where spin was exclusively at the proximal Fe2 atom (Figure S14).

The cathodic processes, $[1]^{+/0}$ found in the CV appeared as irreversible processes at E_{pc} = −1.70 V with a small prereduction event at E_{pc} = −1.47 V (Figure 3). The small reduction event at E_{pc} = −1.47 V did not appear to be an artifact or impurities but is in fact to due to electron-coupled chemical reactions (EC). Furthermore, the two small anodic peaks at E_{pa} = −0.65 and 0.0 V only appear after the potential is swept past the reduction event at −1.70 V. The cathodic

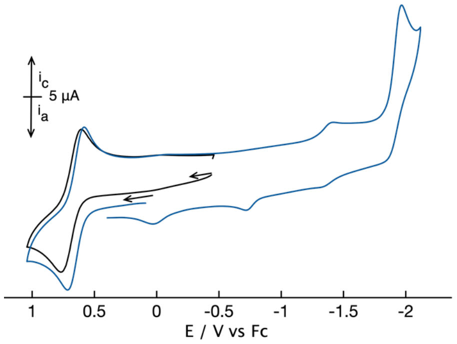

Figure 3. Cyclic voltammetry of $[\mathbf{1}]^+$ in 0.1 M n-$Bu_4N[B(Ar^F)_4]/CH_2Cl_2$.

electrochemical mechanism was further studied by a SEC and DFT analysis.

The UV−vis−NIR SEC spectrum for the reduction process $[\mathbf{1}]^{+/0}$ showed nonisosbestic behavior consistent with an EC mechanism. A new broad, low-energy absorption at λ_{max}/nm (ε/M^{-1} cm^{-1}) = 780 (100) (Figures S11 and S12) appeared. The IR SEC spectrum was used to help understand the cathodic mechanism. The IR SEC spectrum of $[\mathbf{1}]^{+/0}$ at room temperature showed the formation of a new signal at ν_{CO} = 1680 cm^{-1} that appears rapidly (Figure S10), but only after the potential was held at −1.5 V for ∼2−3 min. This large hypsochromic shift for the $\Delta\nu_{CO}$ can be attributed to a change in the binding mode of the CO ligand, where such frequencies are common for bridging CO ligands. Several attempts were made to reduce $[\mathbf{1}]^+$ with reductants such as Na in THF, Na/naphthalene, and $[CoCp_2]$, but no signal at 1680 cm^{-1} could be detected. The reduction of $[\mathbf{1}]^+$ with $[CoCp_2]$ gave a new signal at ν_{CO} = 1779 cm^{-1} consistent with $[CpFe(CO)_2]_2$.

Open-shell DFT calculations were performed on $[\mathbf{1}]^0$ using the same functionals and basis sets as for the closed-shell $[\mathbf{1}]^+$. The spin density analysis is shown in Figure 4, and it shows that a significant amount of spin is located on the Fe (spin up) and the only spin located on the CO ligand has the opposite sign (spin down). The Mulliken spin population on the distal Fe1 is 1.03 and is −0.12 on the C. The electron structure of $[\mathbf{1}]^0$ can be described as a valence tautomer, as shown by the resonance structure in Figure 4, where Fe^I is the dominant resonance structure. A vibrational analysis of $[\mathbf{1}]^+$ and $[\mathbf{1}]^0$ showed a small change in $\Delta\nu_{CO}$, 7 cm^{-1}, which is unexpected on the basis of the additional electron in $[\mathbf{1}]^0$ (see the Supporting Information). The minimal contribution from the π^* orbital in the LUMO of $[\mathbf{1}]^+$ is depicted in Figure 2, and the open-shell calculation placing the majority of the spin density on the Fe center in $[\mathbf{1}]^0$ would be reflected in the small or minimal change in the $\Delta\nu_{CO}$ value. Reduced CO ligands where the CO triple bond is broken is usually only supported by a strong Lewis acid, which generates the carbyne M≡C−O.[17,18]

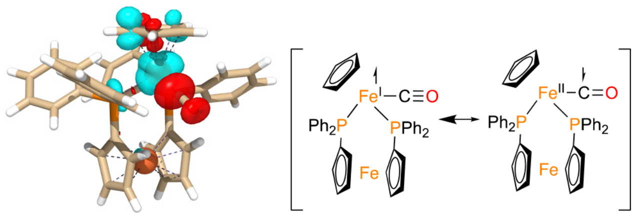

Figure 4. Spin density analysis determined from unrestricted Kohn−Sham orbitals, using the B3LYP/def2-TZVP/J level of theory. Spin up is shown in green, and spin down is shown in red.

The reduction event $[\mathbf{1}]^{+/0}$ was further studied by IR SEC at −30 °C, and the relative intensities of the different species formed during the IR SEC experiments are shown in Figure 5.

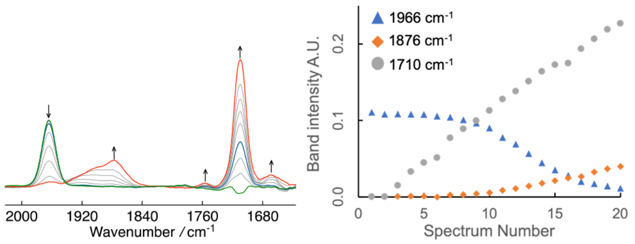

Figure 5. IR SEC spectrum of $[\mathbf{1}]^{+/0}$ at −30 °C in 0.1 M $Bu_4N[B(Ar^F)_4]/CH_2Cl_2$ and the relative intensities of the different signals. Note the *x*-axis denotes the succession of time, but the spectra were not measured at fixed times.

The IR SEC spectrum showed that the signal for $[\mathbf{1}]^+$ at ν_{CO} = 1966 cm^{-1} remained at a similar intensity as the cathodic potential ∼1.5 V was reached, and the signal at ν_{CO} = 1710 cm^{-1} began to increase in intensity (Figure 5). This induction period is unusual behavior; however, it can be explained by the frequency analysis done by DFT calculations on $[\mathbf{1}]^0$ and $[\mathbf{1}]^+$ that showed only a small change in the $\Delta\nu_{CO}$ value, which would explain why the signal at ν_{CO} = 1966 cm^{-1} remained unchanged in intensity over the induction period. The 30 cm^{-1} difference between the ν_{CO} for $[\mathbf{1}]^0$ at −30 °C versus that at 25 °C is not entirely clear at this time; however, the temperature dependence of ν_{CO} has been described in the context of ion pairing,[19] but a close contact with $[B(Ar^F)_4]^-$ is rarely observed.[20]

The new signals at ν_{CO} = 1710 (vs) and 1667 (vw) cm^{-1} and the formation of the signal ν_{CO} = 1876 cm^{-1} can be assigned after considering several possible structures. The first to be considered was the formyl species [CpFe(CHO)(dppf)] ([**1**CHO]), as low-valent iron carbonyls are known to abstract $H^\bullet$ from the solvent or electrolyte.[4,21] The[Rh(por)(CHO)] (por = tetraarylporphyrinato) has a reported $\nu_{C=O}$ = 1700 cm^{-1}; however, this is an unusually high $\nu_{C=O}$, as most metal formyls, including those of iron, have $\nu_{C=O}$ = 1550−1590 cm^{-1}.[4] The structure of [**1**CHO] was calculated and a vibrational analysis was also performed on the optimized structure. The calculated $\Delta\nu_{CO}$ = 336 cm^{-1} between $[\mathbf{1}]^0$ and [**1**CHO] is significantly larger than the observed $\Delta\nu_{CO}$ = 256 cm^{-1}; additionally, no C−H vibrations were observed in the expected region of 2500 cm^{-1}.[21] The formation of a dimer has also been explored and likely explains the IR SEC spectrum.

Two types of dimers were considered on the basis of the IR SEC spectrum. The reduced $[\mathbf{1}]^0$ can dimerize, where the CO ligands can form a new C−C bond similar to the Rh^{II}−CO bond described by Wayland et al., where $[(por)Rh(\mu\text{-}(O{=}C)_2)Rh(por)]$ showed two bands at 1780 and 1769 cm^{-1}.[22−25] The IR spectra of metal α-diketones have been described for complexes with the form $[(OC)_5M(\mu\text{-}(O{=}C)_2)M(CO)_5]$ (M = Re, Mn), and the spectra of such species contained two IR bands for the dionyl μ-$(O{=}C)_2$ ligand that were in the range of 1700−1550 cm^{-1}.[26] While such a dimer, $[CpFe(dppf)]_2(\mu\text{-}(C{=}O)_2)$ (Scheme 3), could be calculated, a vibrational analysis was deemed impractical due to the large number of

Scheme 3. Possible Dimerization Routes after Reduction

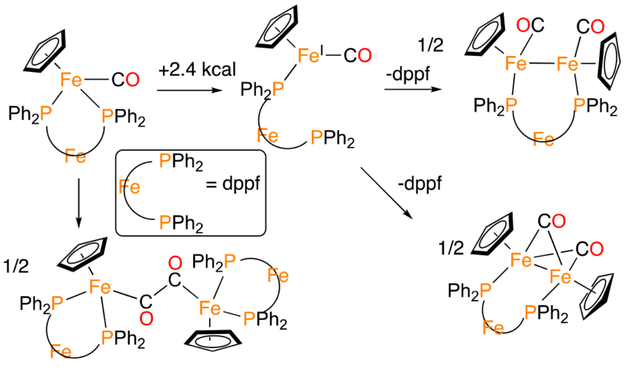

atoms in this complex and the SEC IR spectrum (Figure 5) did not fit with that of the reported (μ-M(O=C)$_2$)M. Thus, this structure was abandoned to pursue the more promising option of dppf displacement and subsequent dimerization.

A second, more feasible dimer based on the bands ν_{CO} = 1710(vs) and 1667(vw) cm^{-1} can be attributed to the formation of a Fe—Fe bond through the displacement of one of the dppf ligands. The energy for the dechelation of dppf from κ^2 to κ^1 was calculated to be ~2.4 kcal mol^{-1} for [**1**]^0 according to a potential energy surface scan (Figure S15). This would allow for the formation of a Fe—Fe bond), where similarly structured complexes [Cp$_2$Fe$_2$(μ-CO)$_2$(μ-P—P)] (P—P = 1,*n*-bis(diphenylphosphino)-C$_n$H$_{2n}$, *n* = 3 (dppp), 2 (dppe), 1 (dppm) have also been described showing ν_{CO}(dppp) = 1725 (vw), 1687 (vs), ν_{CO}(dppe) = 1730 (vw), 1693 (vs),[27,28] and ν_{CO}(dppm) = 1734 (vw), 1690 (s) (Chart 1).[27,28] The complex [Cp$_2$Fe$_2$(μ-CO)$_2$(μ-(P(OEt)$_2$)$_2$O)] showed two bands at 1712 (vs) and 1754 (vw) cm^{-1} (Chart 1).[29] The molecular structure of [Cp$_2$Fe$_2$(μ-CO)$_2$(μ-dppf)] was calculated and is the likely explanation of the bands at ν_{CO} = 1710 (vs) and 1667 (vw) cm^{-1} shown in the IR SEC spectrum at −30 °C (Figure 5); the proposed electrochemical mechanism is shown in Scheme 3.

Chart 1. Reported CpFe(CO) Dimers

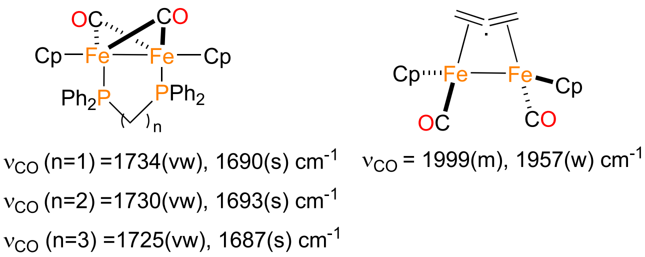

The final bands at 1876 cm^{-1} are thought to be due to the higher energy configuration that contains two terminal CO ligands, [Cp$_2$Fe$_2$(CO)$_2$(μ-dppf)]. The later appearance of the higher energy band is likely due to its weaker intensity, where the similarly structured complex [Cp$_2$Fe$_2$(CO)$_2$(H$_2$CCCH$_2$)] showed ν_{CO} = 1999 (m) (Chart 1).[30] A DFT analysis found that [Cp$_2$Fe$_2$(CO)$_2$(μ-dppf)] is about 20 kcal mol^{-1} higher in energy than [Cp$_2$Fe$_2$(μ-CO)$_2$(μ-dppf)], which would be consistent with less of this species at ν_{CO} = 1876 cm^{-1} being formed during reduction. The terminal CO ligands would also likely be weaker in intensity relative to the bridging counterparts.[30]

■ CONCLUSIONS

The electrochemical behavior of the title complex [CpFe(dppf)(CO)]$^+$ showed a reversible oxidation that occurred at the ferrocenediyl moiety of the dppf ligand and not at the CpFe moiety. The location of this oxidation event was confirmed by IR and UV−vis SEC and was further supported by DFT calculations. The reduction event observed in the cyclic voltammogram is proposed to give an intermediate with significant radical character at the CpFe moiety, and limited spin density is located at the CO ligand. This Fe^I species can undergo dimerization through displacement of one dppf ligand followed by bridging the CO ligands. We are currently investigating the exchange of Cp for Cp* in the iron carbonyl moiety as well as modifications to substituents on the P donors.

■ EXPERIMENTAL SECTION

Information concerning instrumentation and spectrometers can be found in the Supporting Information.

Density functional theory (DFT) calculations were performed using the solid-state structure of [**1**]$^+$. A computational analysis was performed by means of restricted Kohn−Sham density functional theory (DFT) using the B3LYP[31] functional in combination with the D3 dispersion correction[32] with the def2-TZVP and Weigend J auxiliary basis set.[33,34] Geometry optimizations were realized with the ORCA program package with TightSCF convergence (1.0e-7 au).[35] Solvation in CH$_2$Cl$_2$ was modeled using the CPCM solvation model.[36] Open-shell calculations on the structures [**1**]$^{2+}$ and [**1**]^0 were determined by removing or adding 1e$^-$, respectively, and calculations were performed by means of unrestricted Kohn−Sham DFT using the same basis set, functionals, and solvent models as for [**1**]$^+$. For the numerical frequency calculations, only the fast contribution of the solvent response to the molecular vibrations (defined through electronic polarizations) was taken into account.

1,1′-Bis(diphenylphosphino)ferrocene (dppf) (Carbosynth) was crystallized from CH$_2$Cl$_2$/EtOH, and the resulting orange crystals were dried at 50 °C under vacuum. *n*-BuOH (Sigma-Aldrich) was sparged with N$_2$ prior to use. NaB(ArF)$_4$ was synthesized according to a literature procedure.[37]

Tetrabutylammonium tetrakis[3,5-bis(trifluoromethyl)phenyl]-borate (Bu$_4$NB(ArF)$_4$) was made prior to use and passed through a neutral alumina column using CH$_2$Cl$_2$ as eluent to afford a white crystalline solid. The solid is best stored over a drying agent such as CaSO$_4$. The syntheses of [CpFe(CO)$_2$]$_2$ and [CpFe(CO)$_2$I] were done according to a literature procedure,[38] and details can be found in the Supporting Information.

Synthesis of [CpFe(CO)(dppf)]I. [CpFe(CO)$_2$I] (1.00 g, 3.29 mmol) was dissolved in EtOH (80 mL), and dppf (1.82 g, 3.28 mmol) was added to the solution under a flow of nitrogen. The reaction mixture turned dark red after heating to reflux for 120 h or by heating to 160 °C for 2 h in a microwave reactor. This solution was cooled and filtered through Celite. The solvent was reduced to 10 mL under vacuum. Et$_2$O was added to the concentrated solution, and a brown-orange solid precipitated. This solid was collected by filtration and recrystallized using CH$_2$Cl$_2$ overlayered with *n*-hexane, and the final product was dried under vacuum. Yield: 2.11 g (78%). IR (CH$_2$Cl$_2$): ν_{CO} = 1966 cm^{-1}. Anal. Calcd for C$_{40}$H$_{33}$Fe$_2$P$_2$OI·0.25C$_6$H$_{14}$·CH$_2$Cl$_2$: C, 54.49; H, 4.14. Found: C, 54.48; H, 4.16.

Synthesis of [CpFe(CO)(dppf)]B(ArF)$_4$ ([1]$^+$). To a solution of [CpFe(CO)(dppf)]I (508 mg, 0.61 mmol) in MeOH (100 mL) was added NaB(Ar^F)$_4$ (575 mg, 0.65 mmol). The mixture was stirred for 30 min with gentle heating at 40 °C. Demineralized water was added slowly to the cooled solution until no more solid precipitate formed. The pale yellow-brown solid was collected by filtration, washed with demineralized water (3 × 20 mL), and dried under vacuum at 40 °C over $CaSO_4$. ^1H NMR (250 MHz, $CDCl_3$): δ 4.23 (2H), 4.35 (5H), 4.46 (2H), 4.51 (2H), 4.88 (2H), 7.44 + 7.50 (22H), 7.64 (3H), 7.71 (9H). ^{11}B NMR (250 MHz, $CDCl_3$): δ 3.57 ppm. ^{31}P NMR (250 MHz, $CDCl_3$): δ 68.75 ppm. IR (CH_2Cl_2): ν_{CO} = 1966 cm^{-1}. UV−vis (CH_2Cl_2): λ_{max} = 395 nm (2989 mol^{-1} dm^3 cm^{-1}). Anal. Calcd for $C_{72}H_{45}F_{24}FeP_2BO$: C, 55.20; H, 2.89. Found: C, 54.76; H, 3.06.

■ ASSOCIATED CONTENT

Supporting Information

The Supporting Information is available free of charge at https://pubs.acs.org/doi/10.1021/acs.organomet.1c00010.

Experimental details including synthesis of educts and $[\mathbf{1}]^+$, DFT parameters, NMR spectra, and IR and UV−vis spectra not found in the main manuscript (PDF)

XYZ files of $[\mathbf{1}]^+$, $[\mathbf{1}]^0$, $[\mathbf{1}]^{2+}$, and calculated dimeric species (ZIP)

Accession Codes

CCDC 2003561 contains the supplementary crystallographic data for this paper. These data can be obtained free of charge via www.ccdc.cam.ac.uk/data_request/cif, or by emailing data_request@ccdc.cam.ac.uk, or by contacting The Cambridge Crystallographic Data Centre, 12 Union Road, Cambridge CB2 1EZ, UK; fax: +44 1223 336033.

■ AUTHOR INFORMATION

Corresponding Author

Mark R. Ringenberg − *Institut für Anorganische Chemie, Universität Stuttgart, 70569 Stuttgart, Germany;* orcid.org/0000-0001-7585-5757;
Email: mark.ringenberg@iac.uni-stuttgart.de

Authors

Yixian Pan − *Institut für Anorganische Chemie, Universität Stuttgart, 70569 Stuttgart, Germany*
Marc Schnierle − *Institut für Anorganische Chemie, Universität Stuttgart, 70569 Stuttgart, Germany*
Daniel Auweiler − *Institut für Anorganische Chemie, Universität Stuttgart, 70569 Stuttgart, Germany*

Complete contact information is available at: https://pubs.acs.org/10.1021/acs.organomet.1c00010

Notes

The authors declare no competing financial interest.

■ ACKNOWLEDGMENTS

The authors thank Dr. Wolfgang Frey for advice and crystallographic measurements. M.R.R. gratefully acknowledge support by the state of Baden-Württemberg through bwHPC and the German Research Foundation (DFG) through grant no. INST 40/467-1 FUGG for access to the Justus cluster. M.S. and D.A. are funded by the Deutsche Forschungsgemeindschaft SFB1333-C2 and RI2799/3-1, respectively. Funding was provided by Institut für Anorgansiche Chemie, Universität Stuttgart, Stuttgart, Germany.

■ REFERENCES

(1) Hamon, P.; Toupet, L.; Roisnel, T.; Hamon, J.-R.; Lapinte, C. Preparation and Characterization of the Triflate Complex $[Cp^*(dppe)FeOSO_2CF_3]$: A Convenient Access to Labile Five- and Six-Coordinate Iron(I) and Iron(II) Complexes. *Eur. J. Inorg. Chem.* **2020**, *2020*, 84−93.

(2) Hamon, P.; Toupet, L.; Hamon, J.-R.; Lapinte, C. Syntheses and X-ray Crystal Structures of Five- and Six-Coordinated Iron(I) and Iron(II) Complexes with the Same $(\eta^5\text{-}C_5Me_5)Fe(dppe)$ Framework. *Organometallics* **1996**, *15*, 10−12.

(3) Nlate, S.; Guerchais, V.; Lapinte, C. One-electron reduction of the iron carbene complexes $[Fe(Cp^*)(CO)_2(=C(OMe)R)]^+$ (R = H or Me) and hydrogen-atom vs. alkyl-radical transfer in the 19-electron intermediates. *J. Organomet. Chem.* **1992**, *434*, 89−96.

(4) Lapinte, C.; Catheline, D.; Astruc, D. Organometallic electron reservoirs. 15. Electron transfer vs. hydride transfer in the reduction of $[C_5R_5Fe(dppe)(CO)]^+PF_6^-$ (R = H or Me) by lithium aluminum hydride. *Organometallics* **1984**, *3*, 817−819.

(5) Darensbourg, D. J.; Adams, M. J.; Yarbrough, J. C.; Phelps, A. L. Synthesis and Structural Characterization of Potassium Salts of Phosphane-Substituted (Cyclopentadienyl)iron Dicyanides, and Their Use as Bridging Ligands for Copper(I) Phosphane Derivatives. *Eur. J. Inorg. Chem.* **2003**, *2003*, 3639−3648.

(6) Pagnoux-Ozherelyeva, A.; Bolien, D.; Gaillard, S.; Peudru, F.; Lohier, J.-F.; Whitby, R. J.; Renaud, J.-L. Microwave irradiation and flow chemistry for a straightforward synthesis of piano-stool iron complexes. *J. Organomet. Chem.* **2014**, *774*, 35−42.

(7) Hsu, M.-A.; Yen, W.-Y.; Chiang, M. Y. Reaction of $(\eta^5\text{-}C_5H_4R)Fe(CO)_2I$ (R = H, Me) with 1,1′-Bis(diphenylphosphino)ferrocene (Dppf); Crystal Structure of $\{[(\eta^5\text{-}C_5H_5)Fe(CO)(\eta^2\text{-}dppf)]^{\pm}\}$. *J. Chin. Chem. Soc.* **1994**, *41*, 741−747.

(8) Ringenberg, M. Beyond Common Metal-Metal Bonds, κ3 Bis(donor)ferrocenyl→Transition Metal Interaction. *Chem. - Eur. J.* **2019**, *25*, 2396−2406.

(9) Po Yeo, S.; Henderson, W.; Mak, T. W.; Hor, T. S. A. Ruthenocenyl ruthenium bimetallic complexes: electrospray mass spectrometric study of $[RuX(\eta^5\text{-}C_5H_5)(\eta^2\text{-}dppr)]^{n+}$ (dppr = 1,1′-bis(diphenylphosphino)ruthenocene) (X = Cl, n = 0; X = CO, CH3CN, CCHPh, n = 1) and the X-ray crystal and molecular structure of $[Ru(\eta^5\text{-}C_5H_5)(CO)(\eta^2\text{-}dppr)]PF_6$. *J. Organomet. Chem.* **1999**, *575*, 171−181.

(10) Bard, A. J.; Faulkner, L. R. *Electrochemical Methods: Fundamentals and Applications*; Wiley: 2000.

(11) Prins, R. Visible absorption spectra of substituted ferricenium cations. *J. Chem. Soc. D* **1970**, 280b−281.

(12) Sixt, T.; Fiedler, J.; Kaim, W. Iron versus ruthenium oxidation in 1,1′-bis(diphenylphosphino)ferrocene-ruthenium(II) complexes: EPR and spectroelectrochemical evidence. *Inorg. Chem. Commun.* **2000**, *3*, 80−82.

(13) Kowalski, K.; Linseis, M.; Winter, R. F.; Zabel, M.; Záliš, S.; Kelm, H.; Krüger, H.-J.; Sarkar, B.; Kaim, W. Charge Delocalization in a Heterobimetallic Ferrocene-(Vinyl)Ru(CO)Cl$(PiPr_3)_2$ System. *Organometallics* **2009**, *28*, 4196−4209.

(14) Hartmann, S.; Winter, R. F.; Brunner, B. M.; Sarkar, B.; Knodler, A.; Hartenbach, I. (Allenylidene)ruthenium Complexes with Redox-Active Substituents and Ligands. *Eur. J. Inorg. Chem.* **2003**, *2003*, 876−891.

(15) Ohs, A. C.; Rheingold, A. L.; Shaw, M. J.; Nataro, C. Electrochemistry of Group VI Metal Carbonyl Compounds Containing 1,1′-Bis(diphenylphosphino)ferrocene. *Organometallics* **2004**, *23*, 4655−4660.

(16) Berstler, J.; Lopez, A.; Ménard, D.; Dougherty, W. G.; Kassel, W. S.; Hansen, A.; Daryaei, A.; Ashitey, P.; Shaw, M. J.; Fey, N.; Nataro, C. Synthesis and spectroelectrochemistry of transition metal carbonyls with 1,1′-bis(phosphino)metallocene ligands. *J. Organomet. Chem.* **2012**, *712*, 37−45.

(17) Bianconi, P. A.; Williams, I. D.; Engeler, M. P.; Lippard, S. J. Reductive coupling of two carbon monoxide ligands to form a coordinated alkyne. *J. Am. Chem. Soc.* **1986**, *108*, 311−313.

(18) Suess, D. L. M.; Peters, J. C. A CO-Derived Iron Dicarbyne That Releases Olefin upon Hydrogenation. *J. Am. Chem. Soc.* **2013**, *135*, 12580−12583.

(19) Carter, B. T.; Castellani, M. P.; Rheingold, A. L.; Hwang, S.; Longacre, S. E.; Richmond, M. G. Ion-Pairing Thermodynamics for $(\eta^5\text{-pentadienyl})Fe(CO)_2^-$ (Pentadienyl = MeCp, C_5Me_5, C_5Ph_5,

C_9H_7) and X-ray Crystal Structure of [(η^5-C_5Ph_5)Fe$(CO)_2$][PPN]. *Organometallics* **2002**, *21*, 373−379.

(20) Winkler, M.; Schnierle, M.; Ehrlich, F.; Mehnert, K.-I.; Hunger, D.; Sheveleva, A. M.; Burkhardt, L.; Bauer, M.; Tuna, F.; Ringenberg, M. R.; van Slageren, J. Electronic structure of a diiron complex: a multitechnique experimental study of $[(dppf)Fe(CO)_3]^{+/0}$. *Inorg. Chem.* **2021**, DOI: 10.1021/acs.inorgchem.0c03259.

(21) Casey, C. P.; Meszaros, M. W.; Neumann, S. M.; Cesa, I. G.; Haller, K. J. Synthesis and x-ray crystal structures of an analog pair of iron formyl and iron acetyl complexes. *Organometallics* **1985**, *4*, 143−149.

(22) Wayland, B. B.; Woods, B. A.; Coffin, V. L. Evidence for a metallo ketone complex in the reactions of rhodium octaethylporphyrin dimer with carbon monoxide: solution equilibria and spectroscopic studies. *Organometallics* **1986**, *5*, 1059−1062.

(23) Wayland, B. B.; Sherry, A. E.; Poszmik, G.; Bunn, A. G. Formation and reactivity of (tetraarylporphyrinato)rhodium(II) monocarbonyls: bent RhIICO complexes that react like acyl radicals. *J. Am. Chem. Soc.* **1992**, *114*, 1673−1681.

(24) Imler, G. H.; Zdilla, M. J.; Wayland, B. B. Evaluation of the Rh(II)-Rh(II) Bond Dissociation Enthalpy for $[(TMTAA)Rh]_2$ by ^{1}H NMR T2Measurements: Application in Determining the Rh-C(O)-BDE in $[(TMTAA)Rh]_2C = O$. *Inorg. Chem.* **2013**, *52*, 11509−11513.

(25) Imler, G. H.; Bhagan, S.; Coffin, V. L.; Wayland, B. B. Reduction of Carbon Monoxide by $[(TMTAA)Rh]_2$ To Form a Dimetal Ketone Complex. *Inorg. Chem.* **2012**, *51*, 3352−3354.

(26) De Boer, E. J. M.; De With, J.; Meijboom, N.; Orpen, A. G. Structure and reactivity of bridging dimanganese and -rhenium ethane-1,2-dionyl compounds. *Organometallics* **1985**, *4*, 259−264.

(27) Shade, J. E.; Pearson, W. H.; Brown, J. E.; Bitterwolf, T. E. Photochemical Reimer-Tiemann Reactions of $(\eta^5\text{-}C_5H_5)_2Fe_2(\mu\text{-}CO)_2(\mu\text{-}Ph_2PCH_2PPh_2)$ and $(\eta^5\text{-}C_5H_5)_2Fe_2(\mu\text{-}CO)_2(\mu\text{-}Ph_2PCH_2CH_2PPh_2)$. The Molecular structures of $(\eta^5\text{-}C_5H_5)_2Fe_2(\mu\text{-}CO)_2(\mu\text{-}Ph_2PCH_2CH_2PPh_2)$ and $(\eta^5\text{-}CHOC_5H_4)(\eta5\text{-}C_5H_5)Fe_2(\mu\text{-}CO)_2(\mu\text{-}Ph_2PCH_2CH_2PPh_2)$. *Organometallics* **1995**, *14*, 157−161.

(28) Haines, R. J.; Du Preez, A. L. Reactions of metal carbonyl derivatives II. Ditertiary phosphine and arsine derivatives of tetracarbonyldi-π-cyclopentadienyldiiron. *J. Organomet. Chem.* **1970**, *21*, 181−193.

(29) Alvarez, C. M.; Galán, B.; García, M. E.; Riera, V.; Ruiz, M. A.; Bois, C. P-O and C-O Bond Cleavages in the Thermal or Photochemical Reactions of $[Fe_2(\eta^5\text{-}C_5H_5)_2(CO)_4]$ with Tetraethyl Diphosphite. *Organometallics* **2003**, *22*, 3039−3048.

(30) Hoel, E. L.; Ansell, G. B.; Leta, S. Thermal and photochemical rearrangements of a bridging cyclopropylidene ligand to allene in a diiron complex. *Organometallics* **1986**, *5*, 585−587.

(31) Stephens, P. J.; Devlin, F. J.; Chabalowski, C. F.; Frisch, M. J. Ab Initio Calculation of Vibrational Absorption and Circular Dichroism Spectra Using Density Functional Force Fields. *J. Phys. Chem.* **1994**, *98*, 11623−11627.

(32) Grimme, S.; Antony, J.; Ehrlich, S.; Krieg, H. A consistent and accurate ab initio parametrization of density functional dispersion correction (DFT-D) for the 94 elements H-Pu. *J. Chem. Phys.* **2010**, *132*, 154104.

(33) Weigend, F.; Ahlrichs, R. Balanced basis sets of split valence, triple zeta valence and quadruple zeta valence quality for H to Rn: Design and assessment of accuracy. *Phys. Chem. Chem. Phys.* **2005**, *7*, 3297−3305.

(34) Weigend, F.; Häser, M.; Patzelt, H.; Ahlrichs, R. RI-MP2: optimized auxiliary basis sets and demonstration of efficiency. *Chem. Phys. Lett.* **1998**, *294*, 143−152.

(35) Neese, F. The ORCA program system. *Wiley Interdiscip. Rev.: Comput. Mol. Sci.* **2012**, *2*, 73−78.

(36) Takano, Y.; Houk, K. N. Benchmarking the Conductor-like Polarizable Continuum Model (CPCM) for Aqueous Solvation Free Energies of Neutral and Ionic Organic Molecules. *J. Chem. Theory Comput.* **2005**, *1*, 70−77.

(37) Brookhart, M.; Grant, B.; Volpe, A. F. $[(3,5\text{-}(CF_3)_2C_6H_3)_4B]^-[H(OEt_2)_2]^+$: a convenient reagent for generation and stabilization of cationic, highly electrophilic organometallic complexes. *Organometallics* **1992**, *11*, 3920−3922.

(38) Eisch, J. J.; King, R. B. *Organometallic syntheses*; Academic Press: New York, 1965; Vol. *1*.